*Journal of Biomolecular NMR*, **16:** 47–58, 2000.
*KLUWER/ESCOM*



# Refinement of the protein backbone angle ψ in NMR structure calculations

R. Sprangers, M.J. Bottomley, J.P. Linge, J. Schultz, M. Nilges & M. Sattler*
*European Molecular Biology Laboratory, Meyerhofstrasse 1, D-69117 Heidelberg, Germany*

Received 16 September 1999; Accepted 6 December 1999

*Key words:* cross-correlated relaxation, CSA, isotope shifts, ψ angle, structural quality, structure calculation, structure refinement

**Abstract**

Cross-correlated relaxation rates involving the $C^{\alpha}$-$H^{\alpha}$ dipolar interaction and the carbonyl ($C'$) chemical shift anisotropy (CSA) have been measured using two complementary 3D experiments. We show that the protein backbone angle ψ can be directly refined against such cross-correlated relaxation rates ($\Gamma^{H\alpha C\alpha, C'}$) and the three-bond H/D isotope effect on the $C^{\alpha}$ chemical shifts ($^3\Delta C^{\alpha}_{(ND)}$). By simultaneously using both experimental parameters as restraints during NMR structure calculations, a unique value for the backbone angle ψ is defined. We have applied the new refinement method to the α-Spectrin SH3 domain (a β-sheet protein) and to the Sgs1p HRDC domain (an α-helical protein) and show that the quality of the NMR structures is substantially improved, judging from the atomic coordinate precision and the Ramachandran map. In addition, the ψ-refined NMR structures of the SH3 domain deviate less from the 1.8 Å crystal structure, suggesting an improved accuracy. The proposed refinement method can be used to significantly improve the quality of NMR structures and will be applicable to larger proteins.

## Introduction

Improving the quality of three-dimensional (3D) structures is an important objective in biomolecular NMR spectroscopy (Doreleijers et al., 1998). It is especially important to determine the dihedral angles ϕ and ψ in order to define the secondary structure of a protein. While the dihedral angle ϕ can be derived from a number of homo- and heteronuclear $^3$J-coupling constants (Wang and Bax, 1996; Griesinger et al., 1999), it has until recently been difficult to determine the backbone angle ψ from NMR data. Although the $^3J(H^{\alpha}_i,N_{i+1})$ can be measured relatively straightforward, this does not define the backbone angle ψ in a unique manner (Montelione et al., 1989; Seip et al., 1994). Other J-coupling constants that could define ψ via an empirical Karplus curve, like $^3J(N_i,N_{i+1})$ and $^3J(C^{\beta}_i,N_{i+1})$, are very small ($< 0.5$ Hz) and of limited practical use (Griesinger et al., 1999). Thus, during structure calculations the backbone angle ψ is only defined by NOE-derived distance restraints, and the lack of information for ψ often causes poor Ramachandran plots in NMR structures.

A number of approaches, which rely on empirical information, have been proposed for defining the backbone conformation of a protein. For example, the correlation between secondary chemical shifts and the backbone angles ϕ and ψ (Spera and Bax, 1991; Wishart et al., 1991) has been used to refine NMR structures (Celda et al., 1995; Kuszewski et al., 1995). It has also been proposed to use database-derived energy potentials for ϕ and ψ in order to define the backbone conformation (Kuszewski et al., 1996). More recently, database searches have been used to establish an empirical correlation between secondary chemical shifts, sequence homology and high-resolution crystal structures in the Protein Data Bank (PDB) in order to obtain backbone angle restraints for proteins (Cornilescu et al., 1999). However, a potential problem of these methods is that they may bias the backbone conformation towards the structures existing

*To whom correspondence should be addressed. E-mail: sattler@EMBL-Heidelberg.de

in the databases and may even define incorrect backbone angles. Consequently, these methods have to be applied with great care.

Recently, experiments have been introduced in order to measure cross-correlated relaxation rates, which can be related to the backbone angle $\psi$. Pulse sequences have been designed to determine those rates between the $H^{\alpha}$-$C^{\alpha}$ and the $H^{N}$-N dipolar interactions ($\Gamma^{H\alpha C\alpha,H^{N}N}$) (Reif et al., 1997; Yang et al., 1998; Pelupessy et al., 1999) and between the $H^{\alpha}$-$C^{\alpha}$ dipolar interaction and the carbonyl ($C'$) chemical shift anisotropy (CSA) ($\Gamma^{H\alpha C\alpha,C'}$) (Yang et al., 1997, 1998; Chiarparin et al., 1999). The cross-correlated relaxation rates can be measured either in a J-resolved experiment with J-coupling evolution (Reif et al., 1997; Yang et al., 1998) or from the intensity difference of cross peaks in two separate experiments, one with and one without evolution of the heteronuclear $^{1}$J-coupling (Tjandra et al., 1996; Tessari et al., 1997; Chiarparin et al., 1999; Felli et al., 1999; Pelupessy et al., 1999). Here, we have used a new pulse sequence for measuring $\Gamma^{H\alpha C\alpha,C'}$ from the ratio of cross peak intensities in two experiments, which reduces spectral overlap compared to previously proposed experiments.

The cross-correlated relaxation effects have a Karplus-like dependence on the backbone angle $\psi$. However, in contrast to J-couplings, they depend only on NMR parameters which, in principle, can be determined experimentally, i.e. the rotational diffusion correlation time ($\tau_c$) and the $C'$ CSA tensor. Since a given cross-correlated relaxation rate is consistent with up to four different $\psi$ angles, the measurement of a single relaxation rate is not sufficient to define the backbone angle $\psi$ uniquely. It has been proposed to combine the two relaxation rates $\Gamma^{H\alpha C\alpha,H^{N}N}$ and $\Gamma^{H\alpha C\alpha,C'}$ in order to reduce the ambiguities (Yang and Kay, 1998). However, some ambiguities remain because both relaxation rates show a similar degeneracy with respect to the $\psi$ angle. For the same reason, $^{3}J(H_i^{\alpha},N_{i+1})$ cannot be used to resolve the ambiguities of $\Gamma^{H\alpha C\alpha,H^{N}N}$ or $\Gamma^{H\alpha C\alpha,C'}$.

Here we show that this problem can be solved by using additional restraints derived from the three-bond H/D isotope effect on the $C^{\alpha}$ chemical shift, $^{3}\Delta C^{\alpha}_{(ND)}$, for which a correlation with the backbone angle $\psi$ has recently been described (Ottiger and Bax, 1997). The function $^{3}\Delta C^{\alpha}_{(ND)}(\psi)$ is only twofold degenerate with respect to $\psi$ and the observed isotope shifts cluster in two separate regions, for $\alpha$-helical and $\beta$-strand secondary structure. We have refined the $\beta$-structured $\alpha$-Spectrin SH3 domain and the $\alpha$-helical Sgs1p HRDC domain directly against a combination of $\Gamma^{H\alpha C\alpha,C'}$ and $^{3}\Delta C^{\alpha}_{(ND)}$ and show that the $\psi$ angles are defined uniquely. Furthermore, the method is shown to significantly improve the structural quality for both proteins.

## Materials and methods

*NMR samples*

The $^{13}C$,$^{15}N$-labeled NMR samples of the $\alpha$-Spectrin SH3 domain (Blanco et al., 1997) and the Sgs1p HRDC domain (Liu et al., 1999) were prepared as described previously. For the NMR samples, the SH3 domain was dissolved in a 1:1 $H_2O$:$D_2O$ mixture giving a protein concentration of 2.9 mM and the pH was adjusted to 3.4; the HRDC domain was dissolved in a 1:1 $H_2O$:$D_2O$ mixture containing 50 mM NaCl, 0.02% $NaN_3$ and 20 mM sodium phosphate buffer, giving a protein concentration of 1.3 mM at pH 6.5. NMR measurements were done at 303 K and 295 K for the SH3 and HRDC domains, respectively.

*Experimental measurement of* $\Gamma^{H\alpha C\alpha,C'}$

$\Gamma^{H\alpha C\alpha,C'}$ rates were measured using a slightly different version of the pulse sequence given in Figure 1. During the $C^{\alpha} \rightarrow C'$ HMQC step, a delay of $\delta/2$ was used instead of $(\delta - \zeta)/2$ and $(\delta + \zeta)/2$, and for the carbon pulses between a and b the delay $\zeta$ was zero in both the cross and the reference experiment. In that case the relaxation rates were obtained from: $I^{cross}/I^{ref} \approx -\tanh[\Gamma^{H\alpha C\alpha,C'} * (T - \zeta)]$, assuming an approximation (Pelupessy et al., 1999) which introduces an error smaller than 4% for relaxation rates $|\Gamma| < 20\ s^{-1}$ (as is the case for both the SH3 and the HRDC domain). $I^{cross}$ and $I^{ref}$ are the signal intensities in the 'cross' and reference experiment, respectively. In the case of Figure 1, the relaxation rates are obtained correctly from $I^{cross}/I^{ref} = -\tanh[\Gamma^{H\alpha C\alpha,C'} * T]$ without any assumptions.

Cross-correlated relaxation rates were recorded on a Bruker DRX spectrometer operating at a $^{1}H$ frequency of 600 MHz, equipped with a triple-axis gradient unit. For the SH3 domain, the pulse program was executed with 4 (reference, 10 h) and 16 (cross, 40 h) scans per increment and 3D matrices with $44 * 40 * 512$ complex points and acquisition times of 29.2 ($t_1$,$^{15}N$), 26.4 ($t_2$,$^{13}C'$) and 51.2 ($t_3$,$^{1}H$) ms were recorded. For the HRDC domain, the pulse program was executed with 4 (reference, 9.5 h) and 32

(cross, 76 h) scans per increment and 3D matrices with $40 * 40 * 512$ complex points and acquisition times of 30.8 ($t_1$,$^{15}$N), 26.4 ($t_2$,$^{13}$C′) and 51.2 ($t_3$,$^{1}$H) ms were recorded.

For the SH3 domain, the cross-correlated relaxation rates were also measured using the J-resolved experiment described by Yang et al. (1998). The pulse sequence was executed with 16 scans per increment (42 h) and a 3D matrix with $40 * 50 * 512$ complex points and acquisition times of 34.0 ($t_1$,$^{15}$N), 24.6 ($t_2$,$^{13}$C′) and 51.2 ($t_3$,$^{1}$H) ms was recorded.

All spectra were processed using NMRPipe (Delaglio et al., 1995) and analyzed using XEASY (Bartels et al., 1995). For the $t_1$ FID forward-backward linear prediction was applied. Prior to Fourier transformation, time-domain data were multiplied by a 90° shifted, sine-square shaped window function and zero-filled to final sizes of 128, 128 and 1024 points for the processed data in the $\omega_1$, $\omega_2$ and $\omega_3$ dimensions, respectively.

*Experimental measurement of* $^3\Delta C^{\alpha}_{(ND)}$

$^3\Delta C^{\alpha}_{(ND)}$ isotope shifts were measured on a Bruker DRX spectrometer operating at a $^1$H frequency of 500 MHz, equipped with a triple-axis gradient unit using the pulse sequence described by Sørensen and co-workers (Meissner et al., 1998). For both proteins the pulse program was executed with 8 scans per increment (45 h) and two sub-spectra each with $55 * 40 * 512$ complex points and acquisition times of 16.0 ($t_1$,$^{13}$Cα), 27.3 ($t_2$,$^{13}$C′) and 61.4 ($t_3$,$^{1}$H) ms, were obtained.

Spectra were processed using NMRPipe (Delaglio et al., 1995) and peak positions were determined by contour averaging using the program PIPP (Garrett et al., 1991). For the $t_1$ and $t_2$ FIDs linear prediction was applied. Prior to Fourier transformation, time-domain data were multiplied by a 90° shifted, sine-square shaped window function and zero-filled to final sizes of 2048, 128, 1024 points for the processed data in the $\omega_1$, $\omega_2$ and $\omega_3$ dimensions, respectively.

*Karplus coefficients for* $\Gamma^{H\alpha C\alpha,C'}$ *and* $^3\Delta C^{\alpha}_{(ND)}$

In order to refine NMR structures directly against experimental cross-correlated relaxation rates and $^3\Delta C^{\alpha}_{(ND)}$ isotope shifts, Karplus-like potentials in CNS (Brünger et al., 1998) were used. The Karplus coefficients for $\Gamma^{H\alpha C\alpha,C'}$ ($\psi$) in $s^{-1}$ are derived as follows:

$$\begin{aligned}\Gamma(\psi)[s^{-1}] &= \kappa_{dc}/2\{\sigma_x(3\cos^2(\theta_x) - 1) \\ &\quad + \sigma_y(3\cos^2(\theta_y) - 1) \\ &\quad + \sigma_z(3\cos^2(\theta_z) - 1)\} \\ &= A\ \cos^2(\psi + D) \\ &\quad + B\cos(\psi + D) + C\end{aligned} \tag{1a}$$

with:

$$\cos(\theta_\alpha) = a_\alpha + b_\alpha \cos(\psi - 120°)(\alpha = x, y)$$

$$\cos(\theta_z) = a_z + b_z \sin(\psi - 120°)$$

From which we obtain:

$$\begin{aligned}A &= 3\kappa_{dc}/2(\sigma_x b_x^2 + \sigma_y b_y^2 + \sigma_z b_z^2) \\ B &= 3\kappa_{dc}(\sigma_x a_x b_x + \sigma_y a_y b_y) \\ C &= -\kappa_{dc}/2[\sigma_x + \sigma_y + \sigma_z \\ &\quad -3(\sigma_x a_x^2 + \sigma_y a_y^2 + \sigma_z b_z^2)] \\ D &= -120°\end{aligned} \tag{1b}$$

where $\sigma_{x,y,z}$ are the principal components of the C′ CSA tensor, $a_{x,y,z}$ / $b_{x,y,z}$ relate the angles between the $C^\alpha$–$H^\alpha$ dipolar interaction and the principal axes of the CSA tensor ($\theta_{x,y,z}$) to the backbone angle $\psi$ (with $a_x = -0.3095$, $b_x = 0.3531$, $a_y = -0.1250$, $b_y = -0.8740$, $a_z = 0$ and $b_z = -0.9426$) (Yang et al., 1997). $\kappa_{dc} = (4/15)(\mu_0/4\pi)\hbar\gamma_C^2\gamma_H B_0 r^{-3}_{(H\alpha-C\alpha)}\tau_c S^2_{cross}$, $\mu_0$ is the permittivity of free space, $\hbar$ is Planck's constant divided by $2\pi$, $\gamma_i$ is the gyromagnetic ratio of spin i, $B_0$ is the static magnetic field, $r_{ij}$ is the inter-nuclear distance, $S^2_{cross}$ is the generalized order parameter for the cross-correlation between the dipole/dipole and CSA interaction and $\tau_c$ is the rotational diffusion correlation time. $\tau_c$ was determined experimentally from $^{15}$N relaxation experiments ($T_1$, $T_2$ and {$^1$H}-$^{15}$N-NOE) (Farrow et al., 1994) (Wiesner et al., unpublished data) and corrected for the change in viscosity as a result of the different $H_2O$:$D_2O$ ratio.

For $S^2_{cross} = 1$ (residues without local mobility) and a $B_0$ field corresponding to 600 MHz $^1$H frequency, the following Karplus coefficients are obtained for the SH3 domain ($\tau_c = 4.6$ ns) and the HRDC domain ($\tau_c = 8.4$ ns):

$$\begin{aligned}\text{SH3}: &\quad A = 22.7, B = -3.8, \\ &\quad C = -17.0, D = -120° \\ \text{HRDC}: &\quad A = 41.4, B = -6.9, \\ &\quad C = -31.0, D = -120°\end{aligned}$$

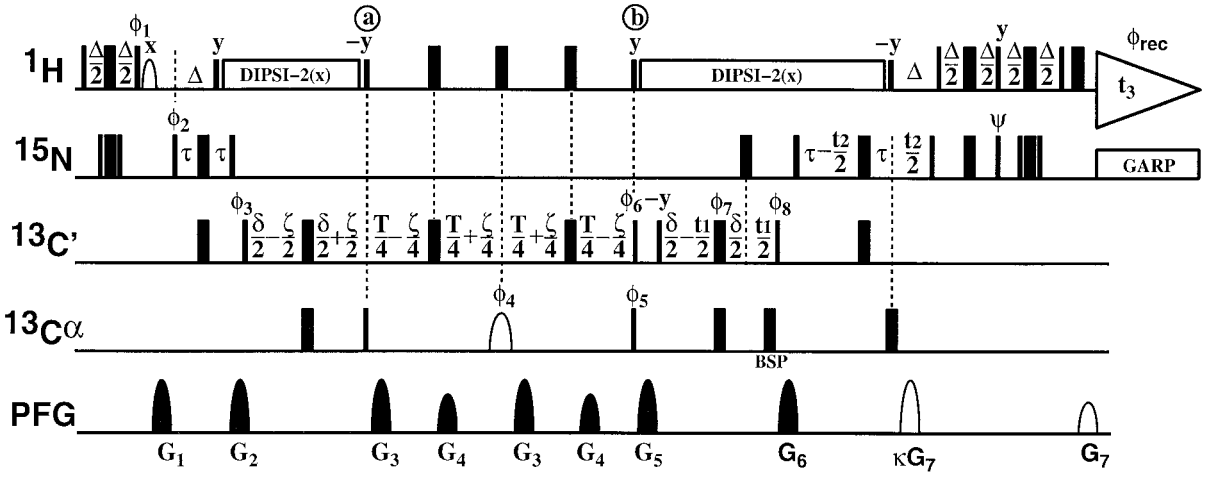


*Figure 1.* Pulse sequence for measuring cross-correlated relaxation rates between the $C^{\alpha}$,$H^{\alpha}$ dipolar interaction and the C′ chemical shift anisotropy. Narrow (wide) bars represent 90° (180°) pulses and are applied along the x-axis, unless indicated otherwise. 90°/180° $^{13}$C pulses are applied as shaped G4/G3-pulses (Emsley and Bodenhausen, 1990) of 400/250 μs duration. Pulses applied to compensate for Bloch–Siegert phase shifts are denoted as 'BSP'. Water flip back is achieved using an $H_2O$ selective Gaussian pulse and 90° (±y) pulses flanking the proton decoupling. Carrier offsets are 4.7 ppm, 118 ppm, 56 ppm and 175 ppm for $^{1}$H, $^{15}$N, $^{13}C^{\alpha}$ and $^{13}$C′, respectively. Delay durations are $\Delta = 5.2$ ms, $\zeta = 0$ ms (reference experiment) or 3.57 ms (cross experiment), T = 28 ms (can be optimized if a $C^{\alpha}$ selective 180° pulse (ϕ4) is applied between a and b in order to refocus the $^{1}J(C^{\alpha},C^{\beta})$ coupling), $\tau = 15$ ms and $\delta = 9.0$ ms. Composite-pulse decoupling fields are applied with strengths of 3.125 kHz and 1.25 kHz for $^{1}$H and $^{15}$N, respectively. The gradient amplitudes and durations are G1 = (0.8 ms, 30.0 G/cm); G2 = (0.8 ms, 42.0 G/cm); G3 = (0.2 ms, 12.0 G/cm); G4 = (0.2 ms, 18.0 G/cm); G5 = (0.8 ms, 36.0 G/cm); G6 = (0.8 ms, 54.0 G/cm) and G7 = (0.8 ms, 5.5 G/cm); κ = 10. For each $t_2$ value κ and ψ are inverted and the corresponding FIDs are stored separately in order to select for echo- and antiecho pathways (Kay et al., 1992; Schleucher et al., 1993). The phase cycling is: $\psi = \pm y$; $\phi_1 = 4(y),4(-y)$; $\phi_2 = 8(x),8(-x)$; $\phi_3 = x + BSP$; $\phi_4 = 16(x), 16(y)$; $\phi_5 = 2(x), 2(-x)$; $\phi_6 = y$ (reference experiment) or x (cross experiment); $\phi_7 = x, y, -x, -y$; $\phi_8 = x + TPPI(t_1)$; $\phi_{rec} = x, 2(-x), x, -x, 2(x), -x, -x,2(x), -x, x, 2(-x), x, -x, 2(x), -x, x, 2(-x), x, x, 2(-x)\ x, -x, 2(x), -x$.

The Karplus coefficients for the isotope shifts $^{3}\Delta C^{\alpha}_{(ND)}$ are:

$$\begin{aligned} {}^{3}\Delta C^{\alpha}_{(ND)}(\psi)[\text{ppb}] &= 22.2\sin(\psi) + 30.1 \\ &= A\cos^2(\psi + D) \\ &\quad + B\cos(\psi + D) + C \end{aligned} \qquad (2)$$

thus, A = 0, B = 22.2, C = 30.1 and D = −90°.

*Structure calculation and evaluation*

The experimentally determined relaxation rates $\Gamma^{H\alpha C\alpha,C'}$ and isotope shifts $^{3}\Delta C^{\alpha}_{(ND)}$ were refined against the potential terms $E_{\Gamma}$ and $E_{\Delta}$ (see text) in CNS (Brünger et al., 1998). For the structure calculations a standard molecular dynamics/simulated annealing (MD/SA) protocol was used corresponding to 10 000 steps at 2000 K, 5000 cooling steps from 2000 K to 1000 K and 2000 cooling steps from 1000 K to 50 K using time steps of 5 fs (Nilges and O'Donoghue, 1998). Optimized force field parameters were used as described (Linge and Nilges, 1999). The potential terms $E_{\Gamma}$ and $E_{\Delta}$ were introduced for $\Gamma^{H\alpha C\alpha,C'}$ and $^{3}\Delta C^{\alpha}_{(ND)}$ restraints during the second cooling phase of the MD/SA protocol using energy constants of $k_{\Gamma} = 0.05$ kcal mol$^{-1}$ s$^{2}$ and $k_{\Delta} = 0.01/0.02$ kcal mol$^{-1}$ ppb$^{-2}$ (SH3/HRDC). The structural quality was assessed using PROCHECK (Laskowski et al., 1996).

## Results and discussion

*Pulse sequence for measuring* $\Gamma^{H\alpha C\alpha,C'}$

We have measured the $\Gamma^{H\alpha C\alpha,C'}$ cross-correlated relaxation rates from the relaxation of $C^{\alpha}$,C′ double- and zero-quantum (DQ/ZQ) coherence during a constant-time delay T using the pulse sequence shown in Figure 1. Note that the pulse sequence is very similar to the experiment proposed recently by Bodenhausen and colleagues, who have also given a detailed theoretical description of this method (Chiarparin et al., 1999). In contrast to the experiments proposed earlier (Yang et al., 1997, 1998), the $^{1}J(C^{\alpha},H^{\alpha})$ coupling is not evolving during $t_1$. Instead, two separate experiments are recorded with different settings for the delay ζ and phase $\phi_6$. For the reference experiment $\phi_6(C') = y$, and $\zeta = 0$, while for the 'cross' experiment $\phi_6(C') = x$, and $\zeta = 1/(2\ ^{1}J(H^{\alpha},C^{\alpha}))$. Thus, the $^{1}J(H^{\alpha},C^{\alpha})$ coupling is refocused in the reference

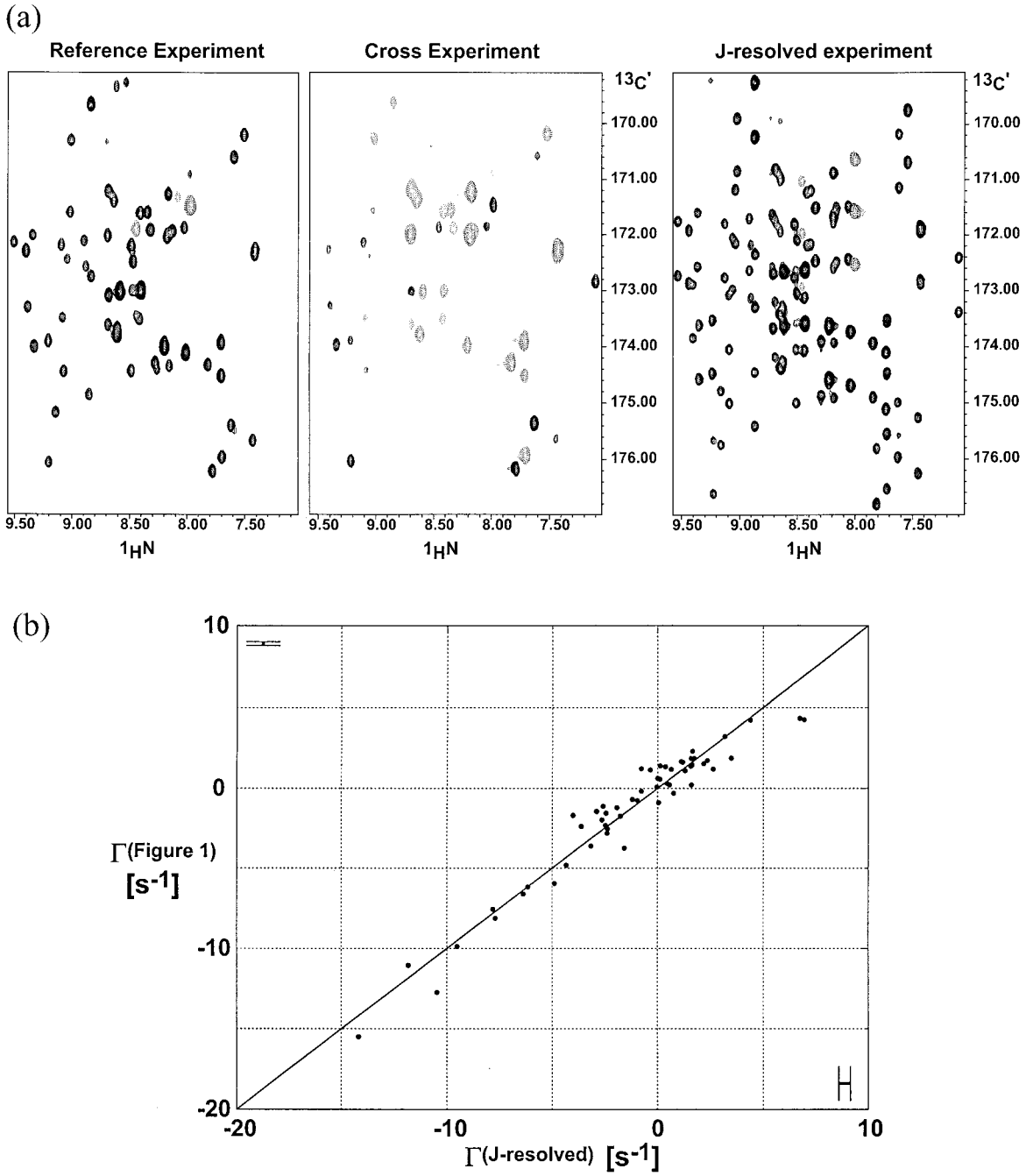


*Figure 2.* (a) Comparison of the $H^{N(i)},C'^{(i-1)}$ projections of 3D spectra obtained with the pulse sequence of Figure 1 (left and middle) and with the pulse sequence described by Yang et al. (1998) (right). Negative peaks are indicated by dotted lines. Due to the $^{1}J(H^{\alpha},C^{\alpha})$ splitting the number of cross peaks is doubled in the spectrum on the right. (b) Comparison of $\Gamma^{H\alpha C\alpha,C'}$ for the SH3 domain obtained using the pulse sequence of Figure 1 and the J-resolved experiment (Yang et al., 1998). The error bars, shown in the corners, indicate the average error from two measurements.

experiment and active for a time $1/(2\,{}^1J(H^\alpha,C^\alpha))$ in the 'cross' experiment. Therefore, in the reference experiment the $4C_y^\alpha C_x' N_z$ operator relaxes under influence of the cross-correlated relaxation during a delay T, while in the 'cross' experiment the scalar ${}^1J(H^\alpha,C^\alpha)$ coupling converts this term into $8C_x^\alpha C_x' N_z H_z$ which is then partially converted into $4C_y^\alpha C_y' N_z$ due to cross-correlated relaxation. In both experiments the desired magnetization at point b in Figure 1 is converted into $4C_z^\alpha C_z' N_z$ and all non-longitudinal magnetization is defocused by gradient 5.

Numerous other cross-correlated relaxation pathways involving dipolar and CSA interactions of the $H^\alpha$, $H^N$, $C^\alpha$ and $C'$ nuclei exist. However, these are either averaged out by the 180° pulses applied between a and b (Figure 1), or the corresponding relaxation rates are much smaller than $\Gamma^{H\alpha C\alpha,C'}$ (Yang et al., 1997; Chiarparin et al., 1999). Therefore, the ratio of the cross peak intensities in the reference and 'cross' experiments is given by: $I^{cross}/I^{ref} = -\tanh[\Gamma^{H\alpha C\alpha,C'} * T]$ and the cross-correlated relaxation rate $\Gamma^{H\alpha C\alpha,C'}$ is obtained from $-\tanh^{-1}(I^{cross}/I^{ref})/T$. Note that variations in ${}^1J(H^\alpha,C^\alpha)$ of 140 ± 8 Hz (Eberstadt et al., 1995) will affect the peak intensities in the cross experiment by less than 0.5%, which translates to a similar change for the extracted relaxation rates.

We have applied the new pulse sequence to the α-Spectrin SH3 domain (Blanco et al., 1997) (Figure 2a) and to the Sgs1p HRDC domain (Liu et al., 1999). The rates $\Gamma^{H\alpha C\alpha,C'}$ measured for the SH3 domain using the experiment of Yang et al. (1998) compared to the new pulse sequence are in excellent agreement within the experimental error (Figure 2b). However, we found the relaxation rates measured with the new pulse sequence to be more reproducible. This could be a result of an imperfect phase correction for Bloch–Siegert phase shifts in the experiment where the heteronuclear ${}^1J$-coupling is resolved in $\omega_1$, which might affect the peak heights of the two doublet lines differently.

When using the pulse sequence shown in Figure 1, the spectral resolution is essentially doubled compared to the J-resolved experiments (Figure 2a). This is advantageous for larger proteins, where the sensitivity of the experiment can be further improved by using a TROSY detection scheme (Pervushin et al., 1997, 1998; Andersson et al., 1998; Czisch and Boelens, 1998) for the final $N \rightarrow H^N$ coherence transfer step. In addition, a $C^\alpha$-selective pulse ($\phi 4$) should then be applied in the middle of T (Yang et al., 1997), such that the delay T can be optimized with respect to sensitivity, depending on the relative size of the auto- and

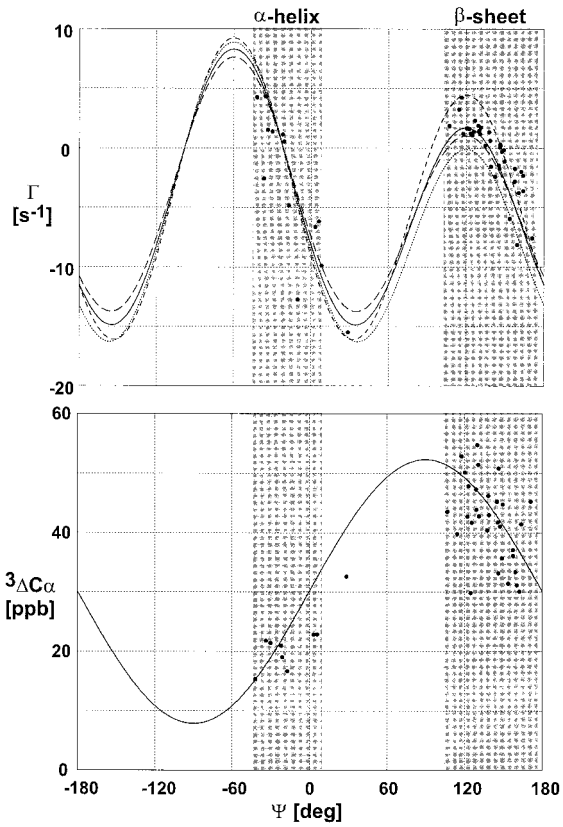


*Figure 3.* Calculated correlation of $\Gamma^{H\alpha C\alpha,C'}$ (top) and ${}^3\Delta C^\alpha_{(ND)}$ (bottom) as a function of the backbone angle ψ for the SH3 domain. For $\Gamma^{H\alpha C\alpha,C'}$, the solid line is calculated with the $C'$ CSA tensor described by Teng et al. (1992). The dotted, dashed and long dashed lines correspond to a 10% larger $\sigma_x$, $\sigma_y$ and $\sigma_z$ component of the CSA tensor, respectively. Note that the cross-correlated relaxation rate scales linearly with the generalized order parameter $S^2_{cross}$ (see Equation 1a). The filled circles are the experimentally determined $\Gamma^{H\alpha C\alpha,C'}$ and ${}^3\Delta C^\alpha_{(ND)}$ plotted against the ψ angles in the crystal structure of the α-Spectrin SH3 domain. Shaded regions indicate the α-helical and β-sheet regions.

cross-correlated relaxation rates. In contrast to the J-resolved experiment, a shorter delay T will not lead to poorer spectral resolution in $\omega_1$, because chemical shift evolution does not take place during this time. In the pulse sequence of Figure 1, $t_1^{max}$ is restricted to δ. However, a longer $t_1^{max}$ can be easily achieved by using semi-constant time chemical shift evolution (Grzesiek and Bax, 1993; Logan et al., 1993).

### *Direct refinement of NMR structures against $\Gamma^{H\alpha C\alpha,C'}$ and ${}^3\Delta C^\alpha_{(ND)}$*

The cross-correlated relaxation rates $\Gamma^{H\alpha C\alpha,H^N N}$ and $\Gamma^{H\alpha C\alpha,C'}$ both provide experimental information about

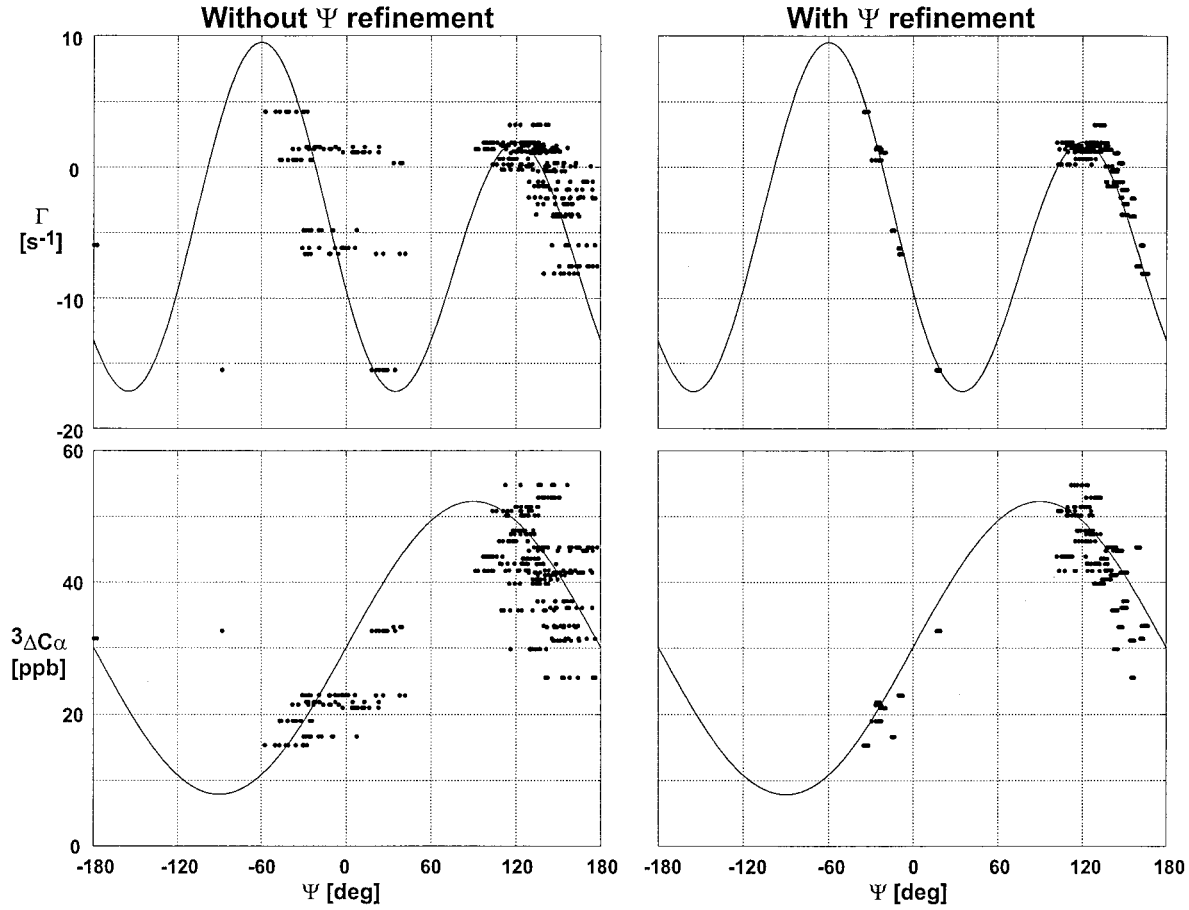


*Figure 4.* Correlation of the experimentally measured cross-correlated relaxation rates (top) and deuterium shifts (bottom) vs. the ψ-angles in the NMR structure ensemble of the SH3 domain without (left) and with (right) ψ-refinement. The filled circles represent the experimentally measured values vs. the ψ angles in the NMR ensemble (10 structures) for all residues where ψ restraints have been applied.

the backbone angle ψ. However, the angle ψ is not defined uniquely even when both relaxation rates are known, because the functions $\Gamma(\psi)$ have a similar degeneracy and phase with respect to ψ (Yang and Kay, 1998). The ψ dependence for $\Gamma^{H\alpha C\alpha,H^NN}$ and $\Gamma^{H\alpha C\alpha,C'}$ (ψ) are given by (Reif et al., 1997; Yang et al., 1997):

$$\Gamma^{H\alpha C\alpha,H^NN}(\psi) = \kappa_{dd}/2(3\cos^2\theta_{dd} - 1) \qquad (3)$$

$$\begin{aligned}\Gamma^{H\alpha C\alpha,C'}(\psi) \;=\; & \kappa_{dc}/2\{\sigma_x(3\cos^2(\theta_x) - 1) \\ & + \sigma_y(3\cos^2(\theta_y) - 1) \\ & + \sigma_z(3\cos^2(\theta_z) - 1)\} \qquad (4)\end{aligned}$$

in which $\kappa_{dd} = (2/5)(\mu_0/4\pi)^2\hbar^2\gamma_C\gamma_N\gamma_H^2 r^{-3}_{(H\alpha-C\alpha)} r^{-3}_{(HN\text{-}N)}\tau_c S^2_{cross}$, $\theta_{dd}$ is the angle between the two dipolar interactions and $\kappa_{dc} = (4/15)(\mu_0/4\pi)\hbar\gamma_C^2\gamma_H B_0 r^{-3}_{(H\alpha-C\alpha)}\tau_c S^2_{cross}$, see Materials and methods section for the other parameters.

Equations 3 and 4 can be rearranged into Karplus-like equations of the form:

$$\Gamma(\psi)[s^{-1}] \;=\; A\cos^2(\psi - D) + B\cos(\psi - D) + C \qquad (5)$$

The Karplus coefficients A, B, C and D depend on the molecular geometry and the dipolar and CSA interactions. For $\Gamma^{H\alpha C\alpha,C'}$ (ψ) they are derived in the Materials and methods section. The H/D isotope shifts $^3\Delta C^\alpha_{(ND)}$ are correlated to the backbone angle ψ by a different Karplus-type relation which is only twofold degenerate and has a different phase:

$$^3\Delta C^\alpha_{(ND)}(\psi)[ppb] \;=\; 22.2\cos(\psi - 90°) + 30.1 \qquad (6)$$

Theoretical Karplus curves for $\Gamma^{H\alpha C\alpha,C'}$ and $^3\Delta C^\alpha_{(ND)}$ are shown in Figure 3. Because the Karplus equations

*Table 1a.* Structural statistics for the SH3 domain

| | # | Unrefined <SA> | ψ-refined <SA> |
|---|---|---|---|
| **Rms deviation (Å) from experimental distance restraints**[a] | | | |
| Unambiguous (total) | 674 | 0.0073±0.0006 | 0.0076±0.0006 |
| Hydrogen bonds | 48 | 0.0060±0.0020 | 0.0062±0.0025 |
| **Rms deviation (°) from experimental torsion angle restraints**[b] | | | |
| Dihedral angles (40 ϕ and 13 $\chi_1$) | 53 | 0.0±0.0 | 0.0±0.0 |
| **Rms deviation from experimental ψ angle restraints**[c] | | | |
| Cross-correlated relaxation rates ($s^{-1}$) | 40 | 4.61±0.79 | 1.22±0.08 |
| Deuterium shifts (ppb) | 40 | 7.52±0.76 | 5.32±0.11 |
| **Deviation from idealized covalent geometry** | | | |
| Bonds (Å) | | 0.0009±0.00004 | 0.0009±0.00003 |
| Angles (°) | | 0.272±0.003 | 0.279±0.003 |
| Impropers (°) | | 0.041±0.018 | 0.0076±0.0007 |
| **Coordinate precision (Å) N, $C^\alpha$, C′ (residues 8–60)**[d] | | | |
| NMR vs. <NMR> | | 0.46±0.11 | 0.38±0.07 |
| NMR vs. X-ray | | 0.66±0.21 | 0.55±0.25 |
| NMR refined vs. unrefined | | 0.22 | |
| **Structural quality** | | | |
| $E_{L.-J.}$[e] | | −222.5±10.8 | −220.7±8.3 |
| % Residues in most favored region of Ramachandran plot[f] | | 80.0±6.0 | 88.0±1.4 |
| % Residues in additionally allowed region | | 17.4±5.3 | 10.0±1.4 |
| # Bad contacts (PROCHECK) | | 0.5±0.70 | 0.2±0.42 |

[a−f]See Table 1b.

for cross-correlated relaxation rates and the H/D isotope shifts introduce different types of ambiguities, a combination of $\Gamma^{H\alpha C\alpha,C'}$ and $^3\Delta C^\alpha_{(ND)}$ can be used to uniquely define ψ. For the α-Spectrin SH3 domain, the experimentally determined relaxation rates $\Gamma^{H\alpha C\alpha,C'}$ and isotope shifts $^3\Delta C^\alpha_{(ND)}$ are plotted against the ψ angles found in the crystal structure (Musacchio et al., 1992) (Figure 3). A very good agreement is found for both $\Gamma^{H\alpha C\alpha,C'}$ and $^3\Delta C^\alpha_{(ND)}$, indicating that they provide a useful measure for the ψ angle. Furthermore, the small rmsd (6.9 ppb) between the experimental $^3\Delta C^\alpha_{(ND)}$ and the isotope shifts calculated based on the 1.8 Å crystal structure of the SH3 domain, is an independent confirmation of Equation 6, which was derived for ubiquitin (Ottiger and Bax, 1997).

The good correlation between the experimental parameters and the crystal structure prompted us to use $\Gamma^{H\alpha C\alpha,C'}$ and $^3\Delta C^\alpha$ as restraints for NMR structure refinement. During the structure calculations Karplus-type potential functions were applied, similar to those used for direct refinement against $^3J(H^N,H^\alpha)$ coupling constants (Kim and Prestegard, 1990; Mierke and Kessler, 1992; Garrett et al., 1994). The following harmonic potentials were used for the cross-correlated relaxation rates $E_\Gamma$ and the H/D isotope shifts $E_\Delta$:

$$E_\Gamma = k_\Gamma\{\Gamma^{H\alpha C\alpha,C'}(\text{exp}) - \Gamma^{H\alpha C\alpha,C'}(\text{calc})\}^2 \quad (7)$$

$$E_\Delta = k_\Delta\{^3\Delta C^\alpha_{(ND)}(\text{exp}) - {}^3\Delta C^\alpha_{(ND)}(\text{calc})\}^2 \quad (8)$$

where (exp) refers to the experimentally determined parameters, and (calc) denotes the values calculated for a given structure using Equations 5 and 6, $k_\Gamma$ and $k_\Delta$ are the energy constants for the cross-correlated relaxation rates and the H/D isotope shifts, respectively.

*Refinement of the backbone angle ψ for an α-helical and a β-sheet protein*

We applied the refinement method to two proteins: the β-sheet SH3 domain and the α-helical HRDC domain. Residues where backbone mobility was indicated by a $\{^1H\}$-$^{15}N$ heteronuclear NOE $< 0.7$ were excluded from the refinement, and restraints were only applied to ψ angles if both parameters were available (40/41 for the SH3/HRDC domain). Small energy constants of $k_\Gamma = 0.05$ kcal $mol^{-1}$ $s^2$ for $\Gamma^{H\alpha C\alpha,C'}$ and $k_\Delta =$

*Table 1b.* Structural statistics for the HRDC domain

| | # | Unrefined <SA> | ψ-refined <SA> |
|---|---|---|---|
| **Rms deviation (Å) from experimental distance restraints**[a] | | | |
| Unambiguous | 1660 | 0.0093±0.0024 | 0.0099±0.0019 |
| Ambiguous | 18 | 0.0031±0.0025 | 0.0042±0.0039 |
| Hydrogen bonds | 34 | 0.0062±0.003 | 0.0080±0.0019 |
| **Rms deviation (°) from experimental torsion angle restraints**[b] | | | |
| Dihedral angles (ϕ) | 47 | 0.0±0.0 | 0.0±0.0 |
| **Rms deviation from experimental ψ angle restraints**[c] | | | |
| Cross-correlated relaxation rates ($s^{-1}$) | 41 | 11.27±0.78 | 1.75±0.06 |
| Deuterium shifts (ppb) | 41 | 8.56±0.31 | 8.16±0.03 |
| **Deviation from idealized covalent geometry** | | | |
| Bonds (Å) | | 0.0012±0.0001 | 0.0013±0.0002 |
| Angles (°) | | 0.310±0.005 | 0.317±0.008 |
| Impropers (°) | | 0.041±0.031 | 0.0064±0.019 |
| **Coordinate precision (Å) N, $C^{\alpha}$, C′ (residues 13–88)**[d] | | | |
| NMR vs. <NMR> | | 0.52±0.12 | 0.48±0.06 |
| NMR refined vs. unrefined | | 0.30 | |
| **Structural quality** | | | |
| $E_{L.-J.}$[e] | | −341.4±14.6 | −349±24.1 |
| % Residues in most favored region of Ramachandran plot[f] | | 89.0±2.2 | 92.0±1.3 |
| % Residues in additionally allowed region | | 10.6±2.2 | 8.0±1.3 |
| # Bad contacts (PROCHECK) | | 0.6±0.51 | 0.1±0.31 |

<SA> is the ensemble of the 10 lowest-energy solution structures. The CNS (Brünger et al., 1998) $E_{Repel}$ function was used to simulate van der Waals interactions with an energy constant of 250 kcal $mol^{-1}$ $Å^{-4}$ using 'PROLSQ' van der Waals radii as described by Linge and Nilges (1999).

[a]Distance restraints were employed with a soft square-well potential (Nilges and O'Donoghue, 1998) using an energy constant of 50 kcal $mol^{-1}$ $Å^{-2}$. Hydrogen bond restraints were derived from slow exchanging amide protons (Blanco et al., 1997; Liu et al., 1999) and applied as 1.8–2.3 Å (H-O) and 2.8–3.3 Å (N-O) distance restraints. No distance restraint was violated by more than 0.4 Å.

[b]ϕ Dihedral angle restraints of $-60° \pm 40°$ or $-120 \pm 40°$ and $\chi_1$ dihedral angle restraints of $-180° \pm 40°$, $-60 \pm 40°$ or $-60 \pm 40°$ were applied using energy constants of 200 kcal $mol^{-1}$ $rad^{-2}$. No dihedral angle restraint was violated.

[c]ψ-restraints were applied as described in the text, using energy constants of 0.05 kcal $mol^{-1}$ $s^2$ for the cross-correlated relaxation rates and 0.01/0.02 kcal $mol^{-1}$ $ppb^{-2}$ for the (SH3/HRDC) $^3\Delta C^{\alpha}_{(ND)}$ isotope shift restraints.

[d]Coordinate precision is given as the Cartesian coordinate rms deviation of the 10 lowest-energy structures with respect to their average structure.

[e]$E_{L.-J.}$ in kcal $mol^{-1}$ is the Lennard-Jones van der Waals energy calculated using the CHARMM PARMALLH6 parameters. $E_{L.-J.}$ was not included in the target function during the structure calculations.

[f]Excluding glycine and proline residues.

$0.01 - 0.02$ kcal $mol^{-1}$ $ppb^{-2}$ for $^3\Delta C^{\alpha}_{(ND)}$ were used in order to account for experimental uncertainties. Importantly, $k_{\Delta}$ is small compared to $k_{\Gamma}$, reflecting the empirical character of $^3\Delta C^{\alpha}_{(ND)}$ (ψ).

The results of the structure refinements of the SH3 domain and the HRDC domain are shown in Figures 4 and 5, respectively; the structural statistics are summarized in Table 1. As can be seen from Figures 4 and 5, there are no ambiguities observed for any of the restrained ψ angles. Furthermore, the residual rmsd violations observed for the relaxation rates decrease significantly in both proteins (Table 1). The small decrease of rmsd violations for the isotope shifts is a result of the smaller force constant used for these restraints. Nevertheless, the residual rmsds are within the same order of magnitude as the rmsd obtained when Equation 6 was derived (Ottiger and Bax, 1997). Note that the residual rmsd should not be smaller in order to prevent over-fitting of the data. A consequence of using a smaller energy constant for the isotope shift restraints is that they mainly serve to resolve the ambi-

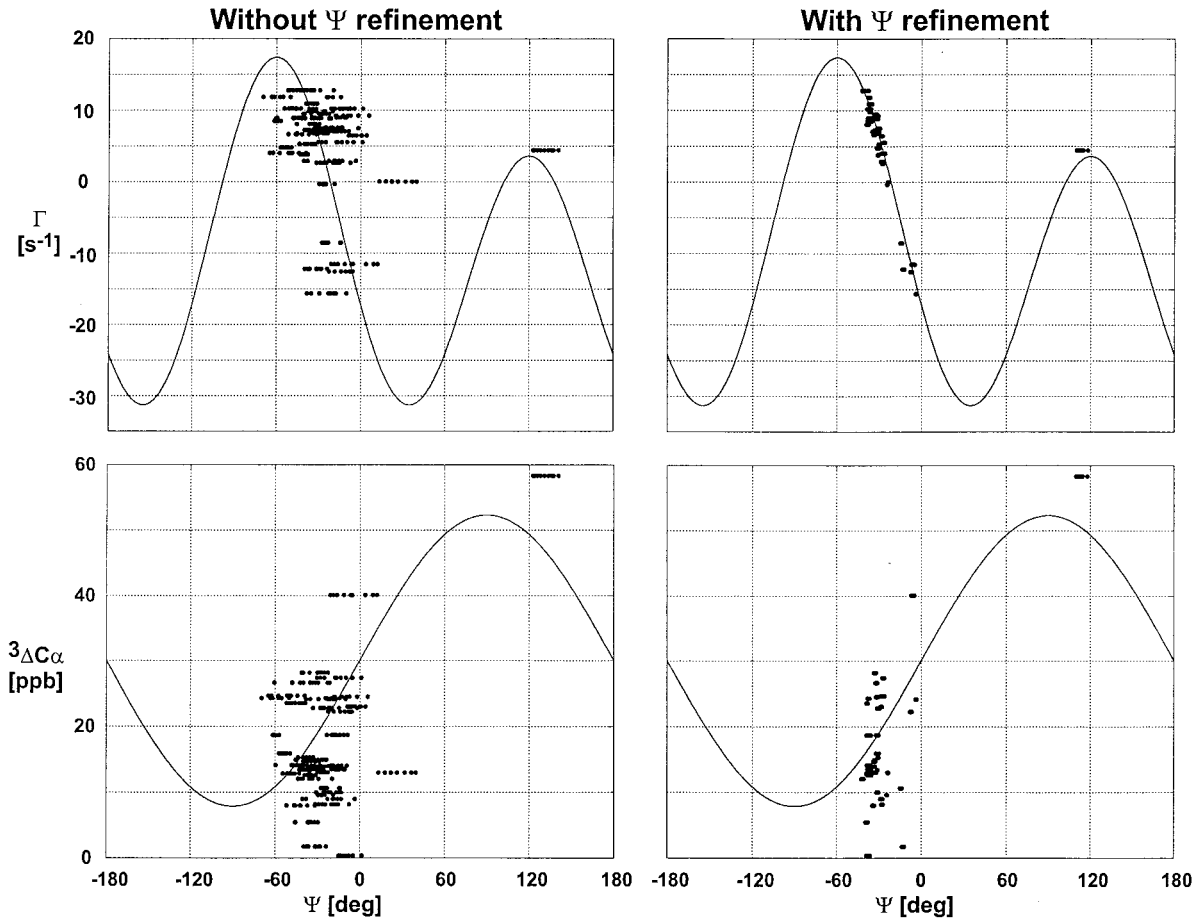


*Figure 5.* Results of the ψ refinement for the HRDC domain (for explanations see Figure 4).

guities of $\Gamma^{H\alpha C\alpha,C'}$ (ψ), and the refinement primarily relies on the cross-correlated relaxation rates.

As expected, the refinement defines the ψ angles more precisely, which is reflected in an improved backbone coordinate precision for the ensembles of NMR structures (17% improvement for the SH3 domain). In addition, the structural quality is substantially improved as indicated by the Ramachandran plot (8% more residues in the most favored region for the SH3 domain). Even for the HRDC domain, which is already very well defined by NOEs, a significant improvement is achieved. Furthermore, for the SH3 domain the backbone rmsd between the crystal structure and the NMR ensemble decreases upon refinement, suggesting an improved accuracy for the ψ-refined structures.

These data demonstrate that NMR structures can be directly refined against a combination of $\Gamma^{H\alpha C\alpha,C'}$ and $^3\Delta C^{\alpha}_{(ND)}$ in order to improve the coordinate precision and structural quality. Note that $\Gamma^{H\alpha C\alpha,H^NN}$ could be used instead of $\Gamma^{H\alpha C\alpha,C'}$ for the ψ refinement. However, at higher $B_0$ fields the $\Gamma^{H\alpha C\alpha,C'}$ rates will be larger than $\Gamma^{H\alpha C\alpha,H^NN}$ and thus can be measured more accurately. Also, a combination of both cross-correlated relaxation rates and the H/D isotope shifts could be used for the ψ refinement, although it is unlikely that the additional, redundant information will lead to a further improvement.

*Further considerations*

It is important to recall that the cross-correlated relaxation rates are influenced by additional parameters. For example, internal mobility affects the correlation function involving the dipole-dipole and CSA interactions, such that $S^2_{cross} < 1$ (Fischer et al., 1997; Brutscher et al., 1998; Ghose et al., 1998). Since the determination of $S^2_{cross}$ is not straightforward, we have excluded residues with local mobility of the

peptide bond. Furthermore, the cross-correlated relaxation rates depend on the size and orientation of the C′ CSA tensor (Figure 3, top). In Equations 4 and 5, a uniform CSA tensor has been assumed for all carbonyls in the protein. However, this might not always be the case, as has recently been shown for the $^{15}$N CSA tensor (Fushman et al., 1998). Additional effects on $\Gamma^{H\alpha C\alpha,C'}$ arise from deviation from isotropic rotational diffusion. In principle, the effect of anisotropic rotational diffusion on the cross-correlated relaxation rates can be calculated (Ghose et al., 1998; Fushman and Cowburn, 1999). However, for small anisotropies of the diffusion tensor these effects are small and can be safely neglected. The good agreement between $\Gamma^{H\alpha C\alpha,C'}$ and the $\psi$ angles which has been observed for a number of proteins (Yang et al., 1998; Chiarparin et al., 1999; this paper) suggests that all effects described above are small. Nevertheless, it is important to use rather weak energy constants for refining against the experimentally measured $\Gamma^{H\alpha C\alpha,C'}$ unless the residue-specific C′ CSA tensors and $S^2_{cross}$ are known.

For larger proteins ($>$ 20 kDa) the HCACO-type experiments used for measuring $^3\Delta C^{\alpha}_{(ND)}$ will suffer from poor signal-to-noise. In that case, secondary $C^{\alpha}$ and $C^{\beta}$ chemical shifts, which depend on $\phi$ and $\psi$, or other observables, which have a different degeneracy with respect to $\psi$ than $\Gamma^{H\alpha C\alpha,C'}$, can be used to resolve the ambiguities of $\Gamma(\psi)$. With this modification the $\psi$ refinement can be applied to larger proteins.

## Conclusions

We have shown that the cross-correlated relaxation rates $\Gamma^{H\alpha C\alpha,C'}$ can be measured reliably from the intensity ratio of cross peaks in two separate 3D experiments. The new pulse sequence can be applied to large molecules by combining it with the TROSY detection scheme and optimizing the constant-time delay for cross-correlated relaxation.

Furthermore, we have demonstrated that NMR structures can be directly refined against a combination of $\Gamma^{H\alpha C\alpha,C'}$ and $^3\Delta C^{\alpha}_{(ND)}$ in order to uniquely define the backbone angle $\psi$. The ambiguities of $\Gamma^{H\alpha C\alpha,C'}$ with respect to $\psi$ are resolved by the additional information available from the H/D isotope shifts $^3\Delta C^{\alpha}_{(ND)}$. Small energy constants are used in order to account for experimental uncertainties and to consider the empirical nature of the correlation between the H/D isotope shifts and the $\psi$ angle.

The $\psi$ refinement leads to substantial improvements in the quality of NMR structures as we have shown for the β-sheet SH3 domain and the α-helical HRDC domain. The atomic coordinate precision and the overall structural quality based on the Ramachandran plot are significantly improved. In addition, the $\psi$-refined NMR structures of the SH3 domain deviate less from the 1.8 Å crystal structure, suggesting an improved accuracy. The method is generally applicable for refining protein NMR structures.

## Acknowledgements

We would like to thank Paco Blanco and Luis Serrano (EMBL Heidelberg) for NMR data and restraint files for the α-Spectrin SH3 domain. M.J.B. is grateful for an EMBO postdoctoral fellowship. R.S. acknowledges support from the ESCOM science foundation. J.P.L. is supported by a Boehringer Ingelheim Ph.D. fellowship. This work has been supported by the DFG (SA 823/1-1).

## References

Andersson, P., Annila, A. and Otting, G. (1998) *J. Magn. Reson.*, **133**, 364–367.

Bartels, C., Xia, T.-H., Billeter, M., Güntert, P. and Wüthrich, K. (1995) *J. Biomol. NMR*, **6**, 1–10.

Blanco, F.J., Ortiz, A.R. and Serrano, L. (1997) *J. Biomol. NMR*, **9**, 347–357.

Brünger, A.T., Adams, P.D., Clore, G.M., DeLano, W.L., Gros, P., Grosse-Kunstleve, R.W., Jiang, J., Kuszewski, J., et al. (1998) *Acta. Crystallogr.*, **D54**, 905–921.

Brutscher, B., Skrynnikov, N.R., Bremi, T., Brüschweiler, R. and Ernst, R.R. (1998) *J. Magn. Reson.*, **130**, 346–351.

Celda, B., Biamonti, C., Arnau, M.J., Tejero, R. and Montelione, G.T. (1995) *J. Biomol. NMR*, **5**, 161–172.

Chiarparin, E., Pelupessy, P., Ghose, R. and Bodenhausen, G. (1999) *J. Am. Chem. Soc.*, **121**, 6876–6883.

Cornilescu, G., Delaglio, F. and Bax, A. (1999) *J. Biomol. NMR*, **13**, 289–302.

Czisch, M. and Boelens, R. (1998) *J. Magn. Reson.*, **134**, 158–160.

Delaglio, F., Grzesiek, S., Vuister, G., Zhu, G., Pfeifer, J. and Bax, A. (1995) *J. Biomol. NMR*, **6**, 277–293.

Doreleijers, J.F., Rullmann, J.A. and Kaptein, R. (1998) *J. Mol. Biol.*, **281**, 149–164.

Eberstadt, M., Gemmecker, G., Mierke, D.F. and Kessler, H. (1995) *Angew. Chem. Int. Ed. Engl.*, **34**, 1671–1695.

Emsley, L. and Bodenhausen, G. (1990) *Chem. Phys. Lett.*, **165**, 469–476.

Farrow, N.A., Muhandiram, R., Singer, A.U., Pascal, S.M., Kay, C.M., Gish, G., Shoelson, S.E., Pawson, T., et al. (1994) *Biochemistry*, **33**, 5984–6003.

Felli, I.C., Richter, C., Griesinger, C. and Schwalbe, H. (1999) *J. Am. Chem. Soc.*, **121**, 1956–1957.

Fischer, M.W.F., Zeng, L., Pang, Y., Hu, W., Majumdar, A. and Zuiderweg, E.R.P. (1997) *J. Am. Chem. Soc.*, **119**, 12629–12642.
Fushman, D. and Cowburn, D. (1999) *J. Biomol. NMR*, **13**, 139–147.
Fushman, D., Tjandra, N. and Cowburn, D. (1998) *J. Am. Chem. Soc.*, **120**, 10947–10952.
Garrett, D.S., Kuszewski, J., Hancock, T.J., Lodi, P.J., Vuister, G.W., Gronenborn, A.M. and Clore, G.M. (1994) *J. Magn. Reson.*, **B104**, 99–103.
Garrett, D.S., Powers, R., Gronenborn, A.M. and Clore, G.M. (1991) *J. Magn. Reson.*, **95**, 214–220.
Ghose, R., Huang, K. and Prestegard, J.H. (1998) *J. Magn. Reson.*, **135**, 487–499.
Griesinger, C., Hennig, M., Marino, J.P., Reif, B., Richter, C. and Schwalbe, H. (1999) In *Modern Techniques in Protein NMR* (N.R. Krishna and L.J. Berliner, Eds.), Plenum Press, New York, NY, pp. 259–367.
Grzesiek, S. and Bax, A. (1993) *J. Biomol. NMR*, **3**, 185–204.
Kay, L.E., Keifer, P. and Saarinen, T. (1992) *J. Am. Chem. Soc.*, **114**, 10663–10665.
Kim, Y. and Prestegard, J.H. (1990) *Proteins*, **8**, 377–385.
Kuszewski, J., Gronenborn, A.M. and Clore, G.M. (1996) *Protein Sci.*, **5**, 1067–1080.
Kuszewski, J., Qin, J., Gronenborn, A.M. and Clore, G.M. (1995) *J. Magn. Reson.*, **B106**, 92–96.
Laskowski, R.A., Rullmann, J.A., MacArthur, M.W., Kaptein, R. and Thornton, J.M. (1996) *J. Biomol. NMR*, **8**, 477–486.
Linge, J.P. and Nilges, M. (1999). *J. Biomol. NMR*, **13**, 51–59.
Liu, Z., Macias, M., Bottomley, M.J., Stier, G., Linge, J., Nilges, M., Bork, P. and Sattler, M. (1999) *Structure*, **7**, 1557–1566.
Logan, T.M., Olejniczak, E.T., Xu, R.X. and Fesik, S.W. (1993) *J. Biomol. NMR*, **3**, 225–231.
Meissner, A., Briand, J. and Sørensen, O.W. (1998) *J. Biomol. NMR*, **12**, 339–343.
Mierke, D. and Kessler, H. (1992) *Biopolymers*, **32**, 1277–1282.
Montelione, G., Winkler, M., Rauenbueler, P. and Wagner, G. (1989) *J. Magn. Reson.*, **82**, 198–204.
Musacchio, A., Noble, M., Pauptit, R., Wierenga, R. and Saraste, M. (1992) *Nature*, **359**, 851–855.
Nilges, M. and O'Donoghue, S.I. (1998) *Prog. NMR Spectrosc.*, **32**, 107–139.
Ottiger, M. and Bax, A. (1997) *J. Am. Chem. Soc.*, **119**, 8070–8075.
Pelupessy, P., Chiarparin, E., Ghose, R. and Bodenhausen, G. (1999) *J. Biomol. NMR*, **13**, 375–380.
Pervushin, K., Riek, R., Wider, G. and Wüthrich, K. (1997) *Proc. Natl. Acad. Sci. USA*, **94**, 12366–12371.
Pervushin, K., Wider, G. and Wüthrich, K. (1998) *J. Biomol. NMR*, **12**, 345–348.
Reif, B., Hennig, M. and Griesinger, C. (1997) *Science*, **276**, 1230–1233.
Schleucher, J., Sattler, M. and Griesinger, C. (1993) *Angew. Chem. Int. Ed. Engl.*, **32**, 1489–1491.
Seip, S., Balbach, J. and Kessler, H. (1994) *J. Magn. Reson.*, **B104**, 172–179.
Spera, S. and Bax, A. (1991) *J. Am. Chem. Soc.*, **113**, 5490–5492.
Teng, Q., Iqbal, M. and Cross, T.A. (1992) *J. Am. Chem. Soc.*, **114**, 5312–5321.
Tessari, M., Vis, H., Boelens, R., Kaptein, R. and Vuister, G.W. (1997) *J. Am. Chem. Soc.*, **119**, 8985–8990.
Tjandra, N., Szabo, A. and Bax, A. (1996) *J. Am. Chem. Soc.*, **118**, 6986–6991.
Wang, A.C. and Bax, A. (1996) *J. Am. Chem. Soc.*, **118**, 2483–2494.
Wishart, D.S., Sykes, B.D. and Richards, F.M. (1991) *J. Mol. Biol.*, **222**, 311–333.
Yang, D., Gardner, K.H. and Kay, L.E. (1998) *J. Biomol. NMR*, **11**, 213–220.
Yang, D. and Kay, L.E. (1998) *J. Am. Chem. Soc.*, **120**, 9880–9887.
Yang, D., Konrat, R. and Kay, L.E. (1997) *J. Am. Chem. Soc.*, **119**, 11938–11940.